Published in final edited form as:
Structure. 2010 May 12; 18(5): 563–570. doi:10.1016/j.str.2010.02.012.

A single mutation promotes amyloidogenicity through a highly promiscuous dimer interface

Francis C. Peterson[1,4], **Elizabeth M. Baden**[1,2], **Barbara A. L. Owen**[3], **Brian F. Volkman**[4], and **Marina Ramirez-Alvarado**[2]

[2] Department of Biochemistry and Molecular Biology, College of Medicine, Mayo Clinic, Rochester, Minnesota 55905, USA

[3] Hematology Research, College of Medicine, Mayo Clinic, Rochester, Minnesota 55905, USA

[4] Department of Biochemistry, Medical College of Wisconsin, Milwaukee, Wisconsin 53226, USA.

Summary

Light chain amyloidosis is a devastating protein misfolding disease characterized by the accumulation of amyloid fibrils that causes tissue damage and organ failure. These fibrils are composed of monoclonal light chain protein secreted from an abnormal proliferation of bone marrow plasma cells. We previously reported that amyloidogenic light chain protein AL-09 adopts an altered dimer while its germline protein (κI O18/O8) forms a canonical dimer observed in other light chain crystal structures. In solution, conformational heterogeneity obscures all NMR signals at the AL-09 and κI O18/O8 dimer interfaces, so we solved NMR structure of two related mutants. AL-09 H87Y adopts the normal dimer interface, but the κI Y87H solution structure presents an altered interface rotated 180° relative to the canonical dimer interface and 90° from the AL-09 arrangement. Our results suggest promiscuity in the light chain dimer interface may promote new intermolecular contacts that may contribute to amyloid fibril structure.

Highlights

- Amyloidogenic light chains adopt altered dimer interface conformations
- Interface mutations destabilizes canonical dimer arrangement
- Dynamic dimer interactions promote new contacts and amyloid formation
- Tyr-to-His substitution at position 87 promotes altered dimer and amyloidogenesis

Introduction

Immunoglobulin light chain amyloidosis (AL) is a rare protein misfolding disease characterized by deposition of amyloid fibrils in the extracellular space of organs and tissues

Contact: Marina Ramirez-Alvarado, Department of Biochemistry and Molecular Biology, College of Medicine, Mayo Clinic, 200 First Street SW, Rochester, Minnesota 55905, Tel. 507 284-2705, Fax 507 284-3383, ramirezalvarado.marina@mayo.edu.

[1]These authors contributed equally to this work

The authors declare no conflicts of interest.

F.C.P. Performed experiments, analyzed data and wrote the manuscript

E.M.B. Performed experiments, analyzed data and wrote the manuscript

B.A.L.O. Performed experiments

B.F.V. Designed research, analyzed data and wrote the manuscript

M.R.A. Designed research, analyzed data and wrote the manuscript

(Gertz and Kyle,1989; Kyle and Gertz,1995). Experimental and bioinformatic comparisons of normal and pathogenic light chains have implicated variations in thermodynamic stability or structural integrity (reviewed in (Baden, et al.,2009)), but specific sequence features responsible for the amyloidogenicity of an immunoglobulin have not been identified.

Typically, immunoglobulins undergo gene rearrangement and somatic hypermutation, followed by the heterotetramerization of two light chains (LCs) and two heavy chains (HCs). The light chain consists of a variable (V_L) and constant (C_L) domain, each adopting the conserved immunoglobulin (Ig) fold. The light chain normally pairs with the corresponding V_H and C_{H1} domains of the heavy chain in a conserved dimer interface. Isolated light chains are commonly found in the circulation (Stevens, et al.,1980), and typically crystallize as homodimers. Amyloid deposits in AL often consist of only the V_L domain (Olsen, et al., 1998), and the V_L–V_L interface in a light chain ("Bence-Jones") dimer involves the same surfaces as the LC-HC variable domains interface (V_L–V_H) (Novotny and Haber,1985).

Several V_L crystal structures of AL proteins have been solved, revealing the conserved Ig fold associating in the canonical Bence-Jones dimer arrangement (Alim, et al.,1999; Bourne, et al., 2002; Epp, et al.,1975; Huang, et al.,1994; Pokkuluri, et al.,1999; Roussel, et al.,1999; Schormann, et al.,1995). However, we recently reported that the crystal structure of AL-09, an AL patient protein characterized in our laboratory, adopts an altered dimer interface that was twisted 90° while its germline counterpart, κI O18/O8, retained the canonical dimer structure (Figure 1A). Though the proteins vary by only seven somatic mutations, AL-09 is significantly more amyloidogenic than κI O18/O8 (Baden, et al.,2008a). Three of the mutations are non-conservative changes (N34I, K42Q, and Y87H) to the κI O18/O8 sequence within or adjacent to the dimer interface. Restorative mutational analysis of the interface residues in AL-09 showed that single mutant AL-09 H87Y restored the canonical dimer interface (Figure 1B and C) (Baden, et al.,2008b). However, a series of reciprocal substitutions in the κI O18/O8 sequence intended to reproduce the altered AL-09 dimer interface (κI Y87H and κI N34I/Y87H) also crystallized in the canonical dimeric arrangement (Figure 1B and C) (Baden, et al.,2008b). Measurements of protein stability and fibril formation kinetics for the restorative and reciprocal mutants demonstrated that histidine at position 87 (as found in AL-09) decreases thermodynamic stability and enhances the amyloidogenicity while a tyrosine at position 87 (as in the germline κI O18/O8 protein) produces the opposite effect. These studies highlighted the importance of tyrosine 87, a residue conserved in more than 95% of κ and λ germline sequences (as found in the VBASE database: http://vbase.mrc-cpe.cam.ac.uk/), but our studies did not reveal an underlying structural link to the amyloidogenicity of AL-09.

To gain further insight into the role of dimer interface mutations in fibril formation, we employed solution NMR to characterize AL-09, κI O18/O8 and their variants. While AL-09 and κI O18/O8 were unsuitable for detailed NMR analysis, we solved the solution structures of the restorative mutant AL-09 H87Y and reciprocal mutant κI Y87H. Surprisingly, κI Y87H adopts a non-canonical dimer interface that was not previously observed in the crystal structures of κI Y87H or AL-09. We also show that while mutation of tyrosine 87 to histidine promotes alternative dimers, mutations at other positions in the interface also contribute to the promiscuous dimer interface of an amyloidogenic Ig light chain by shifting the balance between canonical and non-canonical dimers.

Results

To investigate the role of the dimer interface mutations in fibril formation, we first compared the ^{15}N-^{1}H HSQC spectra of κI O18/O8 and AL-09 (Figure 2A) which are highly dissimilar, with very little overlap in peak positions. While amino acid differences at seven sequence positions would introduce localized chemical shift perturbations, the widespread perturbations

are consistent with the large differences in quaternary structure observed in the crystal structures (Baden, et al.,2008a). Further analysis revealed that nearly half of the expected resonances were absent from each HSQC spectrum and many signals were of reduced intensity due to line broadening. Because both proteins were previously characterized as weak homodimers (AL-09: K_d = 23 μM; κI O18/O8 K_d = 217 μM) (Baden, et al.,2008a), we varied buffer conditions and protein concentration in an unsuccessful effort to improve the HSQC quality and completeness by shifting the monomer-dimer equilibrium. We assigned all residues of κI O18/O8 that could be detected by 3D triple-resonance NMR experiments and found that weak or missing HSQC signals were localized to three discontinuous segments of the primary sequence (Figure 2B). When mapped to surface of a κI O18/O8 monomer, the unassigned residues form a contiguous surface (Figure 2C) that encompasses the distinct but overlapping dimer interfaces described by the crystal structures of κI O18/O8 (Figure 2D) and AL-09 (Figure 2E). Similar results were obtained for AL-09, suggesting that both proteins may exist in a conformational equilibrium that samples multiple dimer interfaces.

To clarify the effect of the Y87H mutation on the structure of the dimer interface, we characterized the AL-09 H87Y restorative and κI Y87H reciprocal mutants by 2D ^{15}N-^{1}H HSQC (Figure 3A). Both spectra were well-dispersed, contained the expected number of cross-peaks with uniform intensities, and lacked the line broadening that we observed for AL-09 and κI O18/O8. We previously reported a dimer K_d = 0.2 μM for AL-09 H87Y (Baden, et al., 2008b), corresponding to a ~100-fold increase in dimer affinity relative to AL-09. To estimate the dimer K_d for κI Y87H, we monitored changes in the HSQC spectrum at protein concentrations from 25 – 800 μM, which were consistent with a two-state monomer-dimer equilibrium in fast exchange on the NMR timescale (Figure S1). Non-linear fitting of the chemical shift perturbations for multiple residues yielded a dimer K_d of 347 ± 57 μM, in reasonable agreement with a K_d (420 ± 5μM) measured under similar conditions by analytical ultracentrifugation (data not shown). Since K_d values for the κI O18/O8 and κI Y87H dimers are within a factor of two, these results suggest the single Y87H mutation in κI O18/O8 restored the NMR spectrum to completeness by restricting the accessible conformations to a simple two-state monomer-dimer equilibrium.

In our earlier structural studies, we reported that AL-09 H87Y and κI Y87H crystallized using the canonical dimer interface observed in most AL proteins (Baden, et al.,2008b). However, this was puzzling because the HSQC spectra of these two proteins (Figure 3A) are just as mismatched as the AL-09 and κI O18/O8 spectra (Figure 2A), and the differences in peak patterns are not easily explained by the 6 remaining somatic mutations or the κI Y87H monomer-dimer equilibrium. To resolve this discrepancy we solved the solution structures of AL-09 H87Y and κI Y87H. Because κI Y87H self-associates relatively weakly (K_d = 347± 57 μM), we were prepared for the NMR data to contain little or no information on the dimer interface. However, we observed strong NOEs that could only arise from intermolecular interactions (Figure S2), and each structure was refined as a homodimer (Table 1). Structural ensembles for each protein displayed low r.m.s.d. values, and uniformly high heteronuclear NOE data values attest to the relative rigidity of backbone within each subunit of the dimer (Figure S3). While the AL-09 H87Y dimer solved by NMR matches the crystal structure, the κI Y87H NMR structure is dramatically different in that one monomer is rotated ~180° relative to the canonical dimer arrangement (Figure 3B).

Intermolecular contacts are significantly reorganized in the altered κI Y87H dimer. Like most other light chain structures, the canonical AL-09 H87Y dimer interface is formed by contacts between one β-sheet of the Ig domain, where symmetry-related strands from each monomer point in the same direction, roughly parallel to the two-fold symmetry axis (Figure 3C). In contrast, the altered dimer conformation in κI Y87H appears slightly elongated and its two-fold axis is reoriented by 90° relative to the canonical dimer (Figure 3D). As a consequence,

β-sheets at the interface are now roughly orthogonal to the two-fold axis, and symmetry-related strands in the opposing monomers are oriented antiparallel relative to each other. The intervening loops also make unique intermolecular contacts in the κI Y87H structure. In the AL-09 H87Y canonical dimer the loop between β-strand C-C' (40s loop) of one monomer packs against the 40s loop of the other monomer, and the complementarity determining region 3 (CDR3) (90s loop) pairs similarly with its counterpart at the opposite end of the dimer interface (Figure 3C). Rotation of the second monomer by ~180° in κI Y87H alters this arrangement and positions the 40s loop of one monomer across from the 90s loop of the second monomer (Figure 3D). Both of these are distinct from the arrangement observed in the crystal structure of AL-09, in which the 90s loop sits at the center of the dimer interface and packs against both the 40s and 90s loops from the other monomer.

To illustrate the striking variation in subunit orientation exhibited by these closely related light chain dimers, we compared the crystal and NMR structures of AL-09 H87Y (Figure 4A and D), κI Y87H (Figure 4B and E), and the crystal structure of AL-09 (Figure 4C) using only one subunit for the alignment. The κI Y87H dimer observed in solution (Figure 4E) is clearly different from the canonical arrangement detected crystallographically (Baden, et al.,2008b) (Figure 4B), which matches the NMR and crystal structures of AL-09 H87Y (Figure 4A and D). Direct comparison of the AL-09, κI O18/O8 and κI Y87H structures shows how variation in the position of the unaligned monomer sweeps like the hands of a clock across the surface of the other monomer at intervals of ~90° (Figure 4F). While a portion of the interface is common to all three dimers, each one forms additional intermolecular contacts distinct from the others, and the combination of all three interfaces correlates well with the region of unassigned NMR signals in κI O18/O8 and AL-09 described above (Figure 2).

Because the structure of κI Y87H solved by NMR is markedly different from the canonical dimer that we previously observed by crystallography (Baden, et al.,2008b), we speculated that the use of 1.2 M citrate as a precipitant, might have destabilized the structure observed by NMR to promote crystallization in the canonical dimer arrangement. Addition of 1 M sodium sulfate (a similarly effective crystallizing anion from the Hofmeister series (Collins,2006)) significantly reduced the number of signals in the 2D ^{1}H-^{15}N HSQC (Figure S4), resulting in a spectrum like those of κI O18/O8 and AL-09 in which interface residues are broadened beyond detection (Figure 2). We concluded that Hofmeister anions like sulfate or citrate create a conformational equilibrium in the κI Y87H quaternary structure by stabilizing the canonical dimer, but that the alternative interface is strongly preferred under less extreme solution conditions.

Collectively, the results for restorative and reciprocal mutants of AL-09 and κI O18/O8 proteins suggest that substitution of histidine for the conserved tyrosine at position 87 plays a major role populating the alternative dimer interfaces observed in the AL-09 crystal structure and the κI Y87H NMR structure. However, our prior thermodynamic analysis indicated that the somatic mutation in position 34 (N34I) also promotes fibril formation, since the κI N34I/Y87H double reciprocal mutant was as thermodynamically unstable and amyloidogenic as AL-09 (Baden, et al.,2008b). To evaluate the effect of an N34I substitution on the dimer interface, we recorded 2D ^{15}N-^{1}H HSQC spectra of κI N34I and κI N34I/Y87H (Figure S5). The κI N34I HSQC contained the expected number of signals with uniform intensity and a pattern similar enough to the AL-09 H87Y HSQC to suggest that κI N34I also favors the canonical dimer interface. A series of spectra collected at concentration ranging from 50-800 μM showed no changes, suggesting that κI N34I is a relatively strong dimer, similar to AL-09 H87Y (K_d = 0.2 μM). In contrast, dimer interface residues were broadened beyond detection in the HSQC of κI N34I/Y87H, just as we observed in κI O18/O8 and AL-09.

Discussion

In a previous study, we discovered that the amyloidogenic human Ig light chain protein AL-09 forms an altered dimer interface in comparison to the corresponding germline protein, κI O18/O8, which adopts the canonical Bence-Jones arrangement. Structural analysis of somatic mutations in the AL-09 sequence showed that restoration of H87 to the germline tyrosine was sufficient to reinstate the canonical dimer, however the Y87H mutation and larger groups of AL-09 mutations were not sufficient to produce an altered dimer. In this study, we show that, while crystallization of the κI Y87H protein in a high salt buffer selected for the canonical dimer, the same protein in less extreme solution conditions preferentially adopts a third, distinct dimer interface. Signals corresponding to the different interfaces are absent from 2D NMR spectra of AL-09, κI O18/O8 and other mutants, suggesting that they interconvert between multiple dimeric structures at rates that lead to extreme line broadening. NMR structural analysis in solution thus provides a more complete picture of the dimer interfaces in AL proteins, and highlights the promiscuous nature of this protein self-interaction.

Dynamic rearrangement of the dimer interface may be a previously unrecognized feature of amyloidogenic light chains. We envision that the global energy landscape for amyloidogenic light chains contains multiple minima representing different dimer conformations. Conformational fluctuations in both monomers allow access to structures that are stabilized by the different dimer interfaces. Dima and Thirumalai have reported aggregation occurring by three parallel routes, where kinetic partitioning leads to parallel assembly pathways early in the aggregation process (Dima and Thirumalai,2002). The role of conformational ensembles in biomolecular recognition has been recently reviewed (Boehr, et al.,2009). The authors propose that molecular interactions can occur through a mechanism called conformational selection, which postulates that all protein conformations pre-exist. In our case, the conformational fluctuations of the interactions between monomers will determine the most favored dimer conformation. After this event, the ensemble undergoes a population shift, redistributing the conformational states. Interconversion between multiple conformational states (e.g. monomer and two or more dimer interfaces) would likely produce the extreme broadening observed in the NMR spectra of AL-09, κI O18/O8, and κI N34I/Y87H.

Our results show that mutations in the κI O18/O8 sequence at positions 34 and 87 work in concert to define both the promiscuity of the dimer interface and the energy of self-association as illustrated in Figure 5A–D. Two of the four possible combinations (I34/Y87 as found in AL-09 H87Y and N34/H87 as found in κI Y87H) are restricted to a single dimer interface (Figure 4A and D), while the other two (I34/H87 and N34/Y87) permit the sampling of multiple arrangements (Figure 4B and E). We noted previously that overall thermodynamic stability in a panel of reciprocal and restorative AL-09 and κI O18/O8 mutants is inversely correlated with amyloidogenic potential (Baden, et al.,2008b). In light of this new evidence for structural heterogeneity at the dimer interface, we searched for structural features common to proteins that form fibrils most rapidly. However, the correlation between dimer promiscuity and amyloidogenicity, as measured by the kinetics of fibril formation, is imperfect (Figure 5B). For example, the κI O18/O8 germline protein is a weak promiscuous dimer (by NMR) that displays slower fibril formation and crystallizes as a canonical dimer.

A clearer distinction between fast and slow rates of fibril formation relies simply on the residue at position 87, where histidine is present in all proteins with fast (<100 h) fibril formation, and tyrosine corresponds to slow (> 200 h) fibril formation (Figure 5E). Proteins with Y87 strongly favor the canonical dimer interface, may not significantly populate the altered dimer interface (Figure 5B and D), and resist fibril formation, while proteins with H87 preferentially form one of the alternative dimers (Figure 5A and C) and are more susceptible to fibril formation.

Each of the alternative dimers creates new intersubunit contacts, for the 40s and 90s loops, as well as for β-strands C' and C" Analysis of the residues involved in the different dimer interfaces populated by AL proteins using the Protein Interfaces, Surfaces and Assemblies (PISA) services (Krissinel and Henrick,2007) showed that while all four interfaces (AL-09, κI O18/O8, AL-09 H87Y and κI Y87H) utilize a very consistent set of residues, residues 49, 50 (located on β-strand C'), 55 (β-strand C"), 56 (loop C"-D) and 87 (β-strand F) are exposed in the AL-09 dimer interface when compared with the other structures. The canonical dimer interface may protect against fibril formation by limiting intermolecular interactions that lower the activation energy for aggregation. Analysis of residues comprising the fibril core for AL proteins is needed to determine which contacts are most amyloidogenic.

Bioinformatic and structural analysis identifies non-conservative mutations at the dimer interface in other AL proteins. Histidine mutations in the λ6a amyloidogenic protein Wil (Wall, et al.,1999) map to the periphery of the dimer interface. When comparing the location of these mutations with H87 in AL-09, it is clear that the Wil mutations occur in different positions of the domain. Using the recently built database of amyloidogenic V_L protein sequences, we found that histidine mutations in dimer interface β-strands (C, F and G) are frequently found in amyloidogenic light chains (Poshusta, et al.,2009), including the mutation characterized in this study, Y87H.

In conclusion, we have shown that the Y87H mutation found in AL-09 alters the free energy landscape for light chain dimer formation and makes non-canonical dimer arrangements accessible. Bioinformatic analysis of the somatic mutations in other AL proteins suggests that other mutations in the dimer interface could lead to similar changes in light chain quaternary structure. We speculate that amyloidogenic light chains populate one of the altered dimers beyond some minimum threshold, even if there is still exchange between different dimers of nearly equal energy, including the canonical dimer interface. Non-canonical dimer arrangements observed in the AL-09 and κI Y87H structures create new intermolecular contacts that may ultimately contribute to amyloid fibril structure.

EXPERIMENTAL PROCEDURES

Protein expression and purification

Recombinant AL-09, AL-09 H87Y, κI O18/O8, κI O18/O8 Y87H, κI O18/O8 N34I and κI O18/O8 N34I/Y87H proteins were expressed in *Escherichia coli* and purified as described previously (Baden, et al.,2008a; Baden, et al.,2008b; McLaughlin, et al.,2006). Isotopically labeled proteins for NMR were produced using M9 media containing [^{15}N]ammonium chloride and [^{13}C]glucose as the sole nitrogen and carbon sources. All proteins were initially purified by FPLC using a HiLoad 16/60 Superdex 75 column on an AKTA FPLC system. AL-09 H87Y and κI Y87H were additionally purified using the Uno-Q anion exchange column. Protein purity was verified by SDS-PAGE and Western blot analysis. Following purification, samples were dialyzed overnight into 10 mM Na_2HPO_4 buffer, pH 7.4, flash frozen and stored at −80° C.

Gel filtration chromatography

Gel filtration was performed using a Bio-Sil size exclusion chromatography HPLC column (Bio-Rad) at 4°C in a buffer containing 50 mM sodium phosphate, pH 6.8, 150 mM NaCl and 10 mM sodium azide on an AKTA FPLC system. Molecular weight standards (Bio-Rad Gel Filtration Standards) were analyzed in the same buffer and consisted of thyroglobulin (670,000), gamma globulin (158,000), ovalbumin (44,000), myoglobin (17,000) and vitamin B_{12} (1350).

Analytical Ultracentrifugation

Sedimentation equilibrium measurements were made on an Optima XL-I equipped with an ultraviolet/interference detection system (Beckman Instruments) as previously described (Baden, et al.,2008a; Owen, et al.,2002; Owen, et al.,2005). Experiments were carried out at 4°C in an ANTi60 rotor until equilibrium was achieved, as judged by scans taken greater than 4 hours apart being superimposable. Each sample was analyzed at multiple rotor speeds (between 10,000 and 15,000 rpm) and at multiple loading concentrations (17, 33, and 50 μM). Data from multiple rotor speeds and multiple concentrations were fit individually and in some cases, simultaneously, using SEDPHAT (Vistica, et al.,2004). Global Species Analysis and fits for self-association models, monomer-dimer, and monomer-dimer-tetramer were used. For κI Y87H, an extinction coefficient of 13,610 was calculated from the amino acid sequence. Vbar was calculated using the program Sednterp (http:/www.jphilo.mailway.com/download.htm) with vbar = 0.6831 for κI Y87H. Buffer density was calculated to be 0.998, also using Sednterp.

NMR spectroscopy

Samples of AL-09, κI O18/O8, κI N34I, κI N34I/Y87H were prepared in buffers containing 10 mM sodium phosphate (pH 6.8), 5-10% (v/v) $^{2}H_{2}O$, and 0.02% (w/v) sodium azide. All 2D ^{15}N-^{1}H HSQC spectra were acquired at 25° C on a Bruker 500 or 600 MHz NMR spectrometer equipped with a triple-resonance CryoProbe™ with NMRPipe (Delaglio, et al., 1995) software. Sample concentrations were 500 μM for AL-09 and κI O18/O8, 800 μM for AL-09 H87Y, κI Y87H, and κI N34I/Y87H and 1.2 mM for κI N34I. Samples for structure determination were prepared in 10 mM MES (pH 6.8) containing 5% (v/v) $^{2}H_{2}O$, and 0.02% (w/v) sodium azide. All structural data was acquired at 25° C using a field strength of 500 or 600 MHz for AL-09 H87Y and κI Y87H, respectively. Each structure determination required a total acquisition time of ~225 hours.

Backbone ^{1}H, ^{15}N and ^{13}C resonance assignments for AL-09 H87Y and κI Y87H were obtained in an automated manner using the program GARANT (Bartels, et al.,1996), with peak lists from 3D HNCO, HNCOCA, HNCOCACB, HNCA, HNCACB, HNCACO, CCONH and 2D ^{15}N-^{1}H HSQC spectra generated manually with XEASY (Bartels, et al.,1995). Side-chain assignments were completed manually from 3D HBHACONH, HCCONH, HCCH-TOCSY, and ^{13}C (aromatic)-edited NOESY-HSQC spectra using XEASY. Chemical shift assignments were >99% complete for each protein.

Structural calculation and analysis

Distance constraints were obtained from 3D ^{15}N-edited NOESY-HSQC and ^{13}C-edited NOESY-HSQC (τ_{mix} = 80 ms). Backbone and dihedral angle constraints were generated from shifts of the $^{1}H\alpha$, $^{13}C\alpha$, $^{13}C^{\beta}$, $^{13}C'$, and ^{15}N nuclei using the program TALOS (Cornilescu, et al.,1999). Initial structures were then generated using the NOEASSIGN module of the torsion angle dynamics program CYANA (Herrmann, et al.,2002) . Initial structures were iteratively refined to eliminate constraint violations. The 20 conformers with the lowest target function were chosen for further refinement by XPLOR-NIH (Schwieters, et al.,2003) using a molecular dynamics protocol in explicit solvent (Linge, et al.,2003). The structures were deposited in the Protein Data Bank (PDB) and the Biological Magnetic Resonance Bank (BMRB). PDB accession numbers for κI Y87H and AL-09 H87Y are 2KQM and 2KQN, respectively. BMRB accession numbers for κI Y87H and AL-09 H87Y are 16606 and 16607, respectively.

Supplementary Material

Refer to Web version on PubMed Central for supplementary material.

Acknowledgments

This work was supported by a grant from the National Institutes of Health (GM071514) and the Mayo Foundation.

References

Alim MA, Yamaki S, Hossain MS, Takeda K, Kozima M, Izumi T, Takashi I, Shinoda T. Structural relationship of kappa-type light chains with AL amyloidosis: multiple deletions found in a VkappaIV protein. Clin Exp Immunol 1999;118:344–348. [PubMed: 10594550]

Baden EM, Owen BA, Peterson FC, Volkman BF, Ramirez-Alvarado M, Thompson JR. Altered dimer interface decreases stability in an amyloidogenic protein. J Biol Chem 2008;283:15853–15860. [PubMed: 18400753]

Baden EM, Randles EG, Aboagye AK, Thompson JR, Ramirez-Alvarado M. Structural insights into the role of mutations in amyloidogenesis. J Biol Chem 2008;283:30950–30956. [PubMed: 18768467]

Baden EM, Sikkink LA, Ramirez-Alvarado M. Light chain amyloidosis - current findings and future prospects. Curr Protein Pept Sci 2009;10:500–508. [PubMed: 19538145]

Bartels C, Billeter M, Güntert P, Wüthrich K. Automated Sequence-specific NMR Assignments of Homologous Proteins using the program GARANT. J. Biomol. NMR 1996;7:207–213.

Bartels C, Xia T-H, Billeter M, Güntert P, Wüthrich K. The Program XEASY for Computer-Supported NMR Spectral Analysis of Biological Macromolecules. J. Biomol. NMR 1995;5:1–10. [PubMed: 7881269]

Boehr DD, Nussinov R, Wright PE. The role of dynamic conformational ensembles in biomolecular recognition. Nat Chem Biol 2009;5:789–796. [PubMed: 19841628]

Bourne PC, et al. Three-dimensional structure of an immunoglobulin light-chain dimer with amyloidogenic properties. Acta Crystallogr D Biol Crystallogr 2002;58:815–823. [PubMed: 11976493]

Collins KD. Ion hydration: Implications for cellular function, polyelectrolytes, and protein crystallization. Biophys Chem 2006;119:271–281. [PubMed: 16213082]

Cornilescu G, Delaglio F, Bax A. Protein backbone angle restraints from searching a database for chemical shift and sequence homology. J Biomol NMR 1999;13:289–302. [PubMed: 10212987]

Delaglio F, Grzesiek S, Vuister GW, Zhu G, Pfeifer J, Bax A. NMRPipe: a multidimensional spectral processing system based on UNIX pipes. J Biomol NMR 1995;6:277–293. [PubMed: 8520220]

Dima RI, Thirumalai D. Exploring protein aggregation and self-propagation using lattice models: phase diagram and kinetics. Protein Sci 2002;11:1036–1049. [PubMed: 11967361]

Epp O, Lattman EE, Schiffer M, Huber R, Palm W. The molecular structure of a dimer composed of the variable portions of the Bence-Jones protein REI refined at 2.0-A resolution. Biochemistry 1975;14:4943–4952. [PubMed: 1182131]

Gertz MA, Kyle RA. Primary systemic amyloidosis--a diagnostic primer. Mayo Clin Proc 1989;64:1505–1519. [PubMed: 2513459]

Herrmann T, Guntert P, Wuthrich K. Protein NMR structure determination with automated NOE assignment using the new software CANDID and the torsion angle dynamics algorithm DYANA. J Mol Biol 2002;319:209–227. [PubMed: 12051947]

Huang DB, Chang CH, Ainsworth C, Brunger AT, Eulitz M, Solomon A, Stevens FJ, Schiffer M. Comparison of crystal structures of two homologous proteins: structural origin of altered domain interactions in immunoglobulin light chain dimers. Biochemistry 1994;33:14848–14857. [PubMed: 7993911]

Krissinel E, Henrick K. Inference of macromolecular assemblies from crystalline state. J Mol Biol 2007;372:774–797. [PubMed: 17681537]

Kyle RA, Gertz MA. Primary systemic amyloidosis: clinical and laboratory features in 474 cases. Semin Hematol 1995;32:45–59. [PubMed: 7878478]

Linge JP, Williams MA, Spronk CA, Bonvin AM, Nilges M. Refinement of protein structures in explicit solvent. Proteins 2003;50:496–506. [PubMed: 12557191]

McLaughlin RW, De Stigter JK, Sikkink LA, Baden EM, Ramirez-Alvarado M. The effects of sodium sulfate, glycosaminoglycans, and Congo red on the structure, stability, and amyloid formation of an immunoglobulin light-chain protein. Protein Sci 2006;15:1710–1722. [PubMed: 16751605]

Novotny J, Haber E. Structural invariants of antigen binding: comparison of immunoglobulin VL-VH and VL-VL domain dimers. Proc Natl Acad Sci U S A 1985;82:4592–4596. [PubMed: 3927286]

Olsen KE, Sletten K, Westermark P. Fragments of the constant region of immunoglobulin light chains are constituents of AL-amyloid proteins. Biochem Biophys Res Commun 1998;251:642–647. [PubMed: 9792827]

Owen BA, Sullivan WP, Felts SJ, Toft DO. Regulation of heat shock protein 90 ATPase activity by sequences in the carboxyl terminus. J Biol Chem 2002;277:7086–7091. [PubMed: 11751892]

Owen BA, et al. (CAG)(n)-hairpin DNA binds to Msh2-Msh3 and changes properties of mismatch recognition. Nat Struct Mol Biol 2005;12:663–670. [PubMed: 16025128]

Pokkuluri PR, Solomon A, Weiss DT, Stevens FJ, Schiffer M. Tertiary structure of human lambda 6 light chains. Amyloid 1999;6:165–171. [PubMed: 10524280]

Poshusta TL, Sikkink LA, Leung N, Clark RJ, Dispenzieri A, Ramirez-Alvarado M. Mutations in specific structural regions of immunoglobulin light chains are associated with free light chain levels in patients with Al amyloidosis. PLoS ONE 2009;4:e5169. [PubMed: 19365555]

Roussel A, Spinelli S, Deret S, Navaza J, Aucouturier P, Cambillau C. The structure of an entire noncovalent immunoglobulin kappa light-chain dimer (Bence-Jones protein) reveals a weak and unusual constant domains association. Eur J Biochem 1999;260:192–199. [PubMed: 10091599]

Schormann N, Murrell JR, Liepnieks JJ, Benson MD. Tertiary structure of an amyloid immunoglobulin light chain protein: a proposed model for amyloid fibril formation. Proc Natl Acad Sci U S A 1995;92:9490–9494. [PubMed: 7568160]

Schwieters CD, Kuszewski JJ, Tjandra N, Clore GM. The Xplor-NIH NMR molecular structure determination package. J Magn Reson 2003;160:65–73. [PubMed: 12565051]

Stevens FJ, Westholm FA, Solomon A, Schiffer M. Self-association of human immunoglobulin kappa I light chains: role of the third hypervariable region. Proc Natl Acad Sci U S A 1980;77:1144–1148. [PubMed: 6767243]

Vistica J, Dam J, Balbo A, Yikilmaz E, Mariuzza RA, Rouault TA, Schuck P. Sedimentation equilibrium analysis of protein interactions with global implicit mass conservation constraints and systematic noise decomposition. Anal Biochem 2004;326:234–256. [PubMed: 15003564]

Wall J, Schell M, Murphy C, Hrncic R, Stevens FJ, Solomon A. Thermodynamic instability of human lambda 6 light chains: correlation with fibrillogenicity. Biochemistry 1999;38:14101–14108. [PubMed: 10529258]

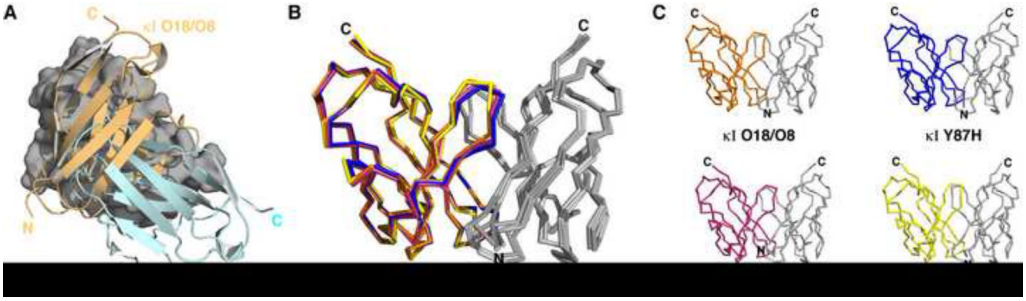

Figure 1. AL-09 contains an altered dimer interface

(A) Superposition of amyloidogenic AL-09 (cyan, PDB ID 2Q1E) and germline κI O18/O8 (orange, PDB ID2Q20) crystal structures. One monomer superimposes well between the two structures (gray surface), but the second monomer of AL-09 is rotated 90° from the canonical dimer interface present in κI O18/O8. (B) Superposition of germline κI O18/O8 (orange) crystal structure with crystal structures of mutants that display the canonical Bence-Jones dimer interface: κI Y87H (blue, PDB ID 3CDF), κI N34I/Y87H (salmon, PDB ID 3CDC) and AL-09 H87Y (yellow, PDB ID 3CDY). (C) Individual representation of the crystal structures of mutants shown in (B).

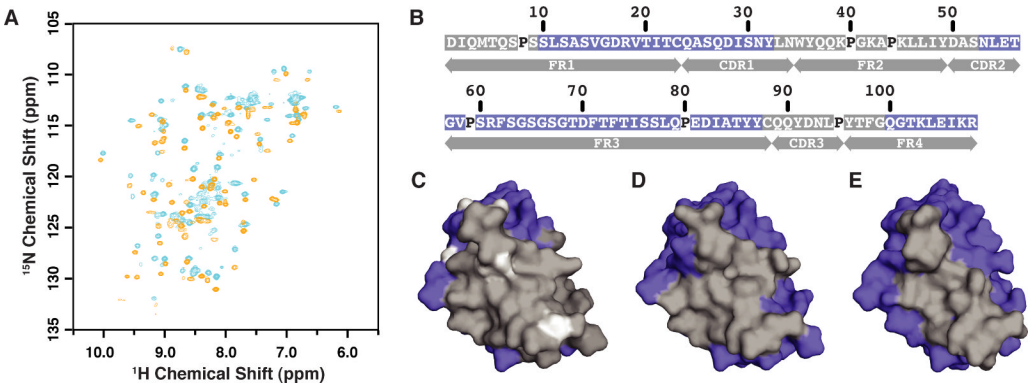

Figure 2. The dimer interfaces of AL-09 and κI O18/O8 are dynamic

(A) Overlay of ^{15}N-^{1}H HSQC spectra for AL-09 (cyan contours) and κI O18/O8 (orange contours). Nonuniform peak intensities, low peak counts, and broadening characterize the spectra of both proteins. (B) Cross-peaks that were unassignable or absent in the ^{15}N-^{1}H HSQC of κI O18/O8 are mapped to its primary sequence. Assigned residues are highlighted in blue and weak/missing residues in gray. Proline residues do not generate cross-peaks in ^{15}N-^{1}H HSQC spectra. (C) Surface representation of the assigned and unassigned cross-peaks in κI O18/O8 colored as in (B). Proline residues are shown in white. (D) Surface representation of the residues that are involved in the κI O18/O8 dimer interface. Residues within 5 Å of the second monomer are colored gray while resides outside the dimer interface are shown in blue. (E) Surface representation of the AL-09 dimer interface, colored as described in (D).

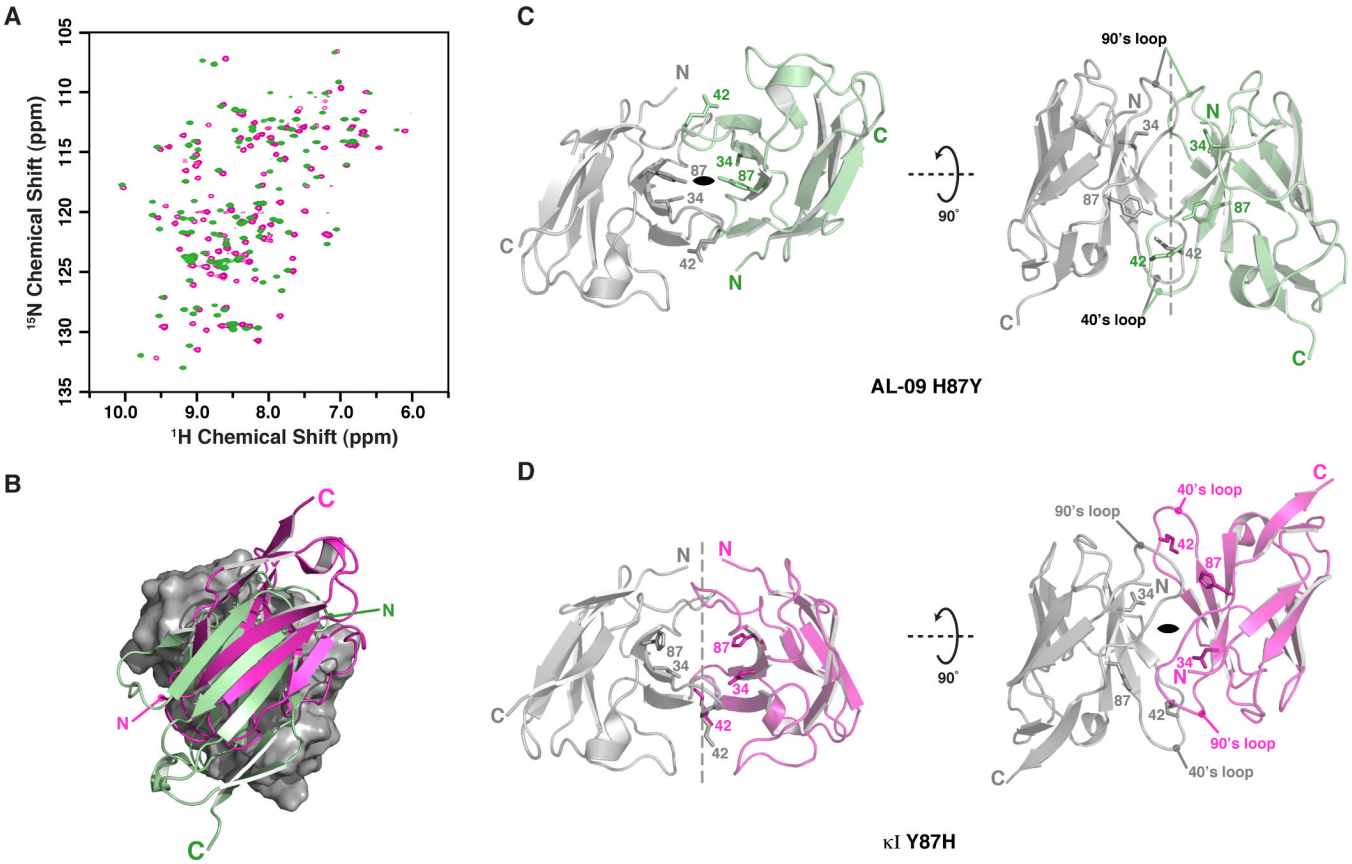

Figure 3. AL-09 H87Y and κI Y87H proteins adopt different dimer interfaces

(A) Overlay of ^{15}N-^{1}H HSQC spectra for AL-09 H87Y (green contours) and κI Y87H (magenta contours). Uniform peak intensities and expected peak counts suggest that restorative and reciprocal mutations restrict each protein to a single dimer interface. (B) Overlay of the AL-09 H87Y (green) and κI Y87H (magenta) NMR structures shows a ~180° rotation of the second monomer. The monomer used for superimposition is shown as a gray surface. (C) Ribbon views of the AL-09 H87Y NMR structure showing the formation of canonical dimer interface, in agreement with the crystal structure of AL-09 H87Y. The two-fold axis of symmetry (dashed line) runs parallel to strands of the β-sheet. Interface residues 34, 42 and 87 are shown as sticks. (D) Ribbon views of κI Y87H NMR structure show an altered dimer interface where the second monomer is rotated by ~180° when compared with AL-09 H87Y. The two-fold axis of symmetry (dashed line) is rotated by 90° in the altered dimer and is now orthogonal to the β-sheet. Subunits in gray are shown in the same orientation in (C) and (D).

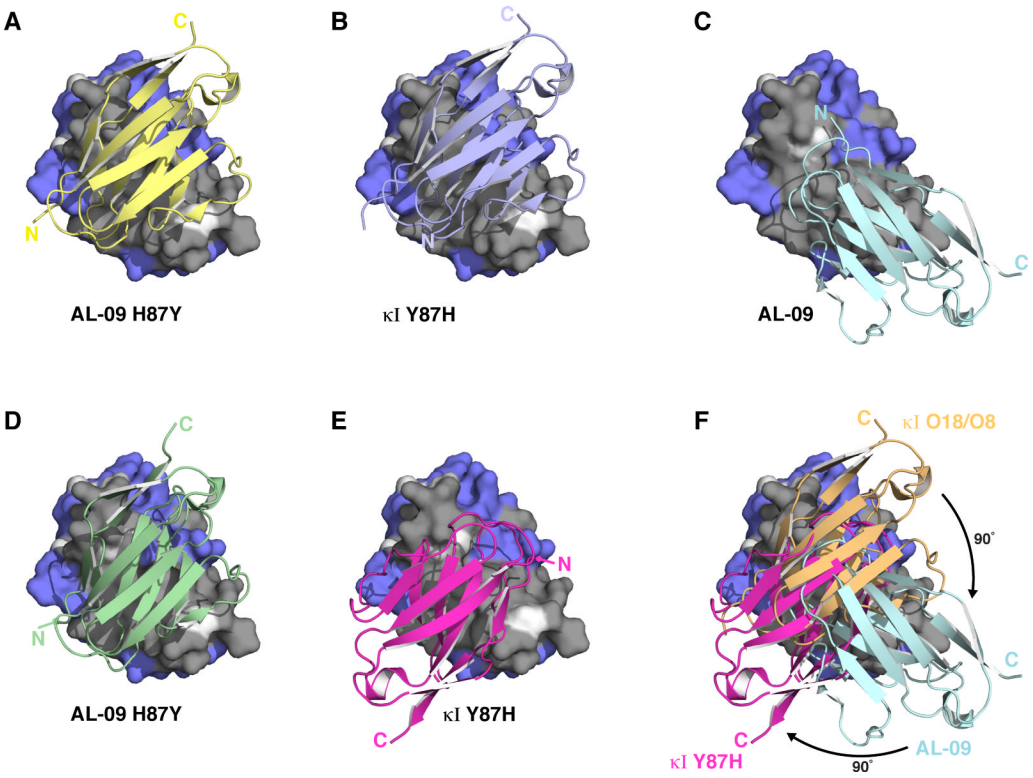

Figure 4. The dimer interfaces in AL-09, κI O18/O8 and their variants access multiple dimer conformations

X-ray crystal structures of (A) AL-09 H87Y, (B) κI Y87H, and (C) AL-09. AL-09 adopts an altered dimer interface that is rotated 90° with respect to canonical dimer present in AL-09 H87Y and κI Y87H. Structures were superimposed using one monomer (surface, colored as describe in Figure 2B) of the homodimer. Solution structures of (D) AL-09 H87Y and (E) κI Y87H. The NMR structure of κI Y87H structure is rotated ~180° with respect to the canonical dimer interface present in the crystallographic structure of κI Y87H shown in (B) and ~90° from the AL-09 dimer interface shown in (C). (F) Overlay of the three unique dimer orientation present in κI O18/O8, AL-09, and the NMR structure of κI Y87H.

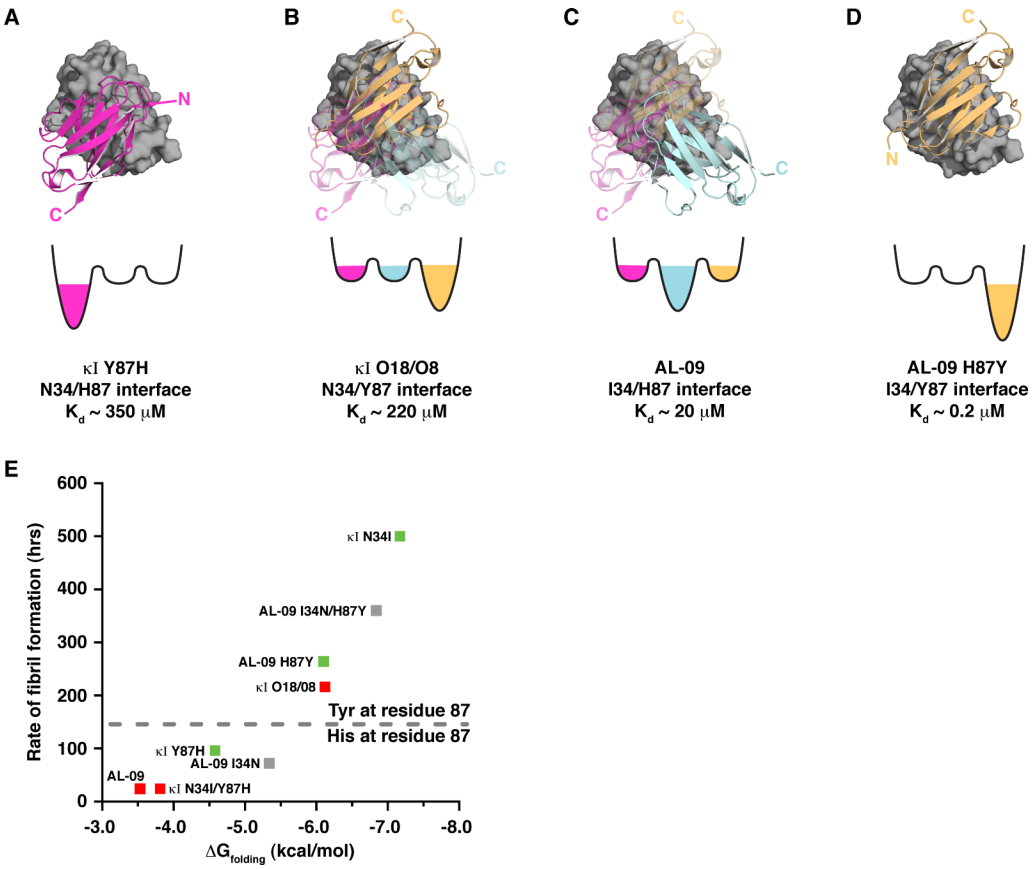

Figure 5. Two residues define the promiscuity of the dimer interface

Somatic mutations at residues 34 and 87 generate four possible combinations of dimer interface residues. (A) Despite having the weakest K_d, the N34/H87 combination in κI Y87H populates only a single interface rotated ~180° relative to the canonical dimer. (B) The N34/Y87 interface in κI O18/O8 permits the sampling of multiple dimer interfaces where the canonical arrangement is slightly lower in energy than the alternatives. (C) AL-09 (I34/H87 interface) samples multiple conformations but prefers an alternative interface rotated 90° relative to the canonical dimer interface. (D) The I34/Y87 pairing in AL-09 H87Y creates the strongest dimer and is restricted mostly to the canonical arrangement, with no significant altered populations present. NMR analysis indicates that another I34/Y87 protein (κI N34I) exhibits similar behavior. (E) Rates of fibril formation are inversely correlated with $\Delta G_{folding}$. Mutation of Y87 to histidine stabilizes an altered dimer interface and promotes faster rates of fibril formation. HSQC analysis was used to categorize each protein as single-state (green) or promiscuous dimers (red); others were not determined (gray).

Table I

Structural Statistics for the 20 conformers of AL-09 H87Y and κI Y87H

Experimental constraints		AL-09 H87Y PDB ID 2KQN	κI Y87H PDB ID 2KQM
Distance constraints			
Intermonomer		77	24
Long		1027	1214
Medium [1<(i–j)≤5]		265	340
Sequential [(i–j)=l]		394	489
Intraresidue [i=j]		341	410
Total		2104	2477
Dihedral angle constraints (Total)		149	151
ϕ		74	73
ψ		75	78
Average atomic R.M.S.D. to the mean structure (Å)			
Dimer (3-106 of Monomers A and B)			
Backbone (C^{α}, C′, N)		0.54 ± 0.13	0.54 ± 0.14
Heavy atoms		0.84 ± 0.10	0.82 ± 0.10
Monomer A (3-106)			
Backbone (C^{α}, C′, N)		0.37 ± 0.07	0.34 ± 0.05
Heavy atoms		0.75 ± 0.06	0.69 ± 0.04
Monomer B (3-106)			
Backbone (C^{α}, C′, N)		0.37 ± 0.06	0.33 ± 0.08
Heavy atoms		0.75 ± 0.04	0.69 ± 0.06
Deviations from idealized covalent geometry			
Bond lengths	RMSD (Å)	0.017	0.018
Torsion angle violations	RMSD (°)	1.4	1.3
WHATCHECK quality indicators			
Z-score		0.21 ± 0.12	0.79 ± 0.12
RMS Z-score			
Bond lengths		0.77 ± 0.01	0.80 ± 0.02
Bond angles		0.63 ± 0.01	0.65 ± 0.01
Bumps		0 ± 0	0 ± 0
Lennard-Jones energy[a] (kJ mol^{-1})		−5,967 ± 87	−6,109 ± 63
Constraint violations			
NOE distance[b]	Number > 0.5 Å	0 ± 0	0 ± 0
NOE distance[c]	RMSD (Å)	0.015 ± 0.001	0.014 ± 0.001
Torsion angle violations	Number ° 5 °	0.0 ± 0	0.0 ± 0
Torsion angle violations	RMSD (°)	0.670 ± 0.072	0.850 ± 0.050
Ramachandran statistics (% of all residues)			
Most favored		84.9 ± 1.2	89.2 ± 1.0

Experimental constraints	AL-09 H87Y PDB ID 2KQN	κI Y87H PDB ID 2KQM
Additionally allowed	12.6 ± 1.2	8.3 ± 1.0
Generously allowed	0.7 ± 0.4	0.2 ± 0.4
Disallowed	1.8 ± 0.4	2.3 ± 0.5

[a] Nonbonded energy was calculated in XPLOR-NIH.

[b] The maximum distance violation was 0.27 and 0.28 Å for AL-09 H87Y and κI Y87H, respectively.

[c] The maximum angle violation was 4.6° and 4.0° for AL-09 H87Y and κI Y87H, respectively.